

# Wall and Support Interference Corrections of NASA Common Research Model Wind Tunnel Tests in JAXA

Masataka Kohzai<sup>1</sup>, Makoto Ueno<sup>2</sup>, Seigo Koga<sup>3</sup>, Norikazu Sudani<sup>4</sup>  
*Japan Aerospace Exploration Agency, Chofu, Tokyo, 182-8522, Japan*

In the JAXA 2m x 2m Transonic Wind Tunnel (JTWT), there have been more needs of wind tunnel users for high measurement accuracy to develop aircraft and launch vehicles with high performance. Integration modern test techniques of the JTWT have to be established. Wind tunnel tests with an 80% scaled NASA Common Research Model (CRM) are conducted to validate our results. Errors of balance output due to balance calibration temperature are confirmed. The test section Mach number, the clear tunnel buoyancy, the wall interference, and the upflow angle corrections are integrated and applied to the CRM wind tunnel tests data in the JTWT. Support interference effects with results of CFD with support and CFD without support are investigated. Moreover, our wall interference correction results and support interference effects are compared with wall interference corrections of the NASA National Transonic Facility (NTF) and the NASA Ames 11-ft Wind Tunnel, and support interference effects of the NTF. Thus, these results show that aerodynamic data, which are not affected by wind tunnel, can be estimated more precisely by the application of the balance calibration matrix, fundamental wind tunnel interference corrections, and the support interference correction appropriately.

## Nomenclature

$b$	=	wing span
$c$	=	wing mean aerodynamic cord
$C_D$	=	drag coefficient
$C_{D\_buoyancy}$	=	buoyancy correction coefficient to be subtracted from drag coefficient
$C_L$	=	lift coefficient
$C_m$	=	pitching moment coefficient
$C_p$	=	pressure coefficient
$C_{p\_center}$	=	pressure coefficient along the centerline in the wind tunnel measured by the short centerline probe
$M_{pc}$	=	plenum chamber Mach number
$P_0$	=	stagnation pressure
$P_{pc}$	=	plenum chamber pressure
$Re_c$	=	Reynolds number based on aerodynamic cord
$S_{Model}$	=	model cross sectional area
$S_{ref}$	=	model reference area
$X$	=	model station
$X_{nose}$	=	model nose station
$X_{tail}$	=	model tail station
$\alpha$	=	angle of attack
$\eta$	=	fraction of wing semi-span

<sup>1</sup> Researcher, Wind Tunnel Technology Center, Member AIAA.

<sup>2</sup> Associate Senior Researcher, Wind Tunnel Technology Center, Member AIAA.

<sup>3</sup> Engineer, Wind Tunnel Technology Center, Member AIAA.

<sup>4</sup> Senior Researcher, Wind Tunnel Technology Center, Member AIAA.

## I. Introduction

THE JAXA 2m x 2m Transonic Wind Tunnel (JTWT) has one of the largest test sections of transonic facilities in Japan, and is the only facility in this country which produces continuous transonic flows. This wind tunnel has been used for testing of most of aircraft and launch vehicles developed in Japan and for fundamental aerodynamic researches. To develop aircraft and launch vehicles with high performance, there have been more needs of wind tunnel users for high measurement accuracy.

The Aerodynamic forces measured in the wind tunnel are affected by the test section walls and the sting-strut system. Aerodynamic data on the flight condition need to be predicted to design aircraft, so that these effects in the wind tunnel data need to be corrected precisely. In the JTWT, the panel method<sup>1</sup> is normally used to correct the wall interference, and comparisons between the results corrected by the method and by Mokry's method<sup>2</sup>, which is other wall interference correction method, are conducted. The applicability of the methods to the JTWT is not, however, investigated sufficiently, because the correction amount of a standard model in the wind tunnel has been negligibly small. Moreover, the test section walls, the sting, the sting-strut system, and the model influence one another. Relations of these effects have been analyzed by comparisons between wind tunnel tests (WTT) data and computational fluid dynamics (CFD) data using a calibration model<sup>3,4,5</sup>.

The AIAA Applied Aerodynamics Technical Committee has initiated a series of Drag Prediction Workshops<sup>6</sup>. The goal of the workshops is to assess state-of-the-art computational methods as practical aerodynamic tools for aircraft force and moment prediction of industry relevant geometries, with the focus being on drag prediction. The Drag Prediction Workshops (DPW) are designed to serve as an impartial forum for evaluating the effectiveness of existing computational Navier-Stokes solvers and modeling techniques. The fourth drag prediction workshop (DPW-IV), held in June of 2009, was a set of blind calculations. For this workshop, the calculations were conducted on a brand new model called the NASA Common Research Model (CRM). The aerodynamic design of the CRM was taken the lead on by The Boeing Company, while model design, fabrication, and testing of the CRM were taken the lead on by the NASA FA/SFW Project<sup>7</sup>. As the validation data for the calculations presented in the DPW-IV, experimental investigations of the CRM have been completed in the NASA National Transonic Facility (NTF) and the NASA Ames 11-ft Wind Tunnel (Ames 11-ft)<sup>8</sup>. Force and moment, surface pressure and surface flow visualization data were obtained at chord Reynolds numbers of 5 million.

We have to establish integration modern test techniques for the JTWT. Then, wind tunnel tests with an 80% scaled CRM have been conducted to validate our results. The size of the model manufactured newly is approximately 130% of our standard model size, so that effects of the wall interference are relatively high. The results are compared with calculated results of the CFD and experimental results of the NTF and the Ames 11-ft Wind Tunnel<sup>9</sup>. In this study, facility description of the JTWT and the 80% scaled CRM are described. It is confirmed that errors of balance outputs due to the balance calibration temperature. Test section Mach number, clear tunnel buoyancy, wall interference, and upflow corrections are integrated and applied to NASA CRM wind tunnel tests data in the JTWT. Next, support interference effects are investigated by CFD analysis. Results of the CRM with support and the CRM without support are compared. Moreover, our wall interference correction results and support interference effects are compared with wall interference corrections of the NTF and the Ames 11-ft, and support interference effects of the NTF.

## II. Facility Description

The JTWT is a closed-circuit and continuously operating facility (Figure 1). The test section is 2m wide, 2m high, and about 4m long. The Mach number range is from 0.1 to 1.4. For subsonic flows, the Mach number is controlled by the rotation of the main blower. For transonic flows, the suction blower is used to bleed the test section of airflow to avoid flow choking. The stagnation pressure ( $P_0$ ) can be varied from 50 to 140 kPa, and stagnation temperature can be varied from 308 to 338 K within the accuracy of 1 K. However, the range of temperature control depends on outside air temperature, because the cooling system is a heat exchanger using water. The maximum Reynolds number is about 20 million per meter (Table 1). In the JTWT, the plenum chamber Mach number ( $M_{pc}$ ), which is calculated with the  $P_0$  and the plenum chamber pressure ( $P_{pc}$ ), is conventionally used to control and determine the test section Mach number. For subsonic flow, the Mach number is controlled by the rotation of the main blower. For transonic flow, the suction blower is used to bleed air from the test section to the plenum chamber for the purpose of avoiding flow choking.

We have four test sections, which we call "carts". Cart #4 is for full-span model and the most frequently used cart. In Cart#4, all four walls are perforated and have holes perpendicular to the walls with a perforation of 20%. We usually have two runs in a day. One day operation consists of two runs, and one run is for about two hours in the morning, and the other run is for about three hours in the afternoon.

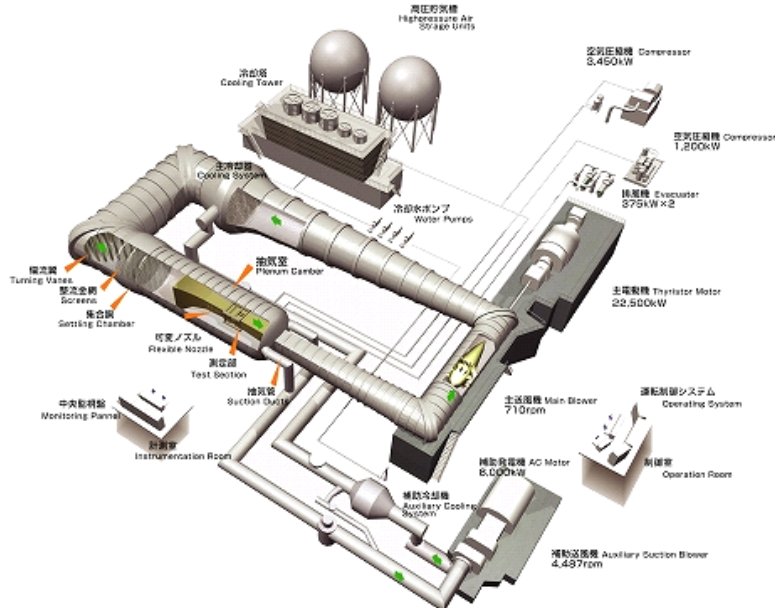


Figure 1. Schematic of the JTWT.

Table 1. Specification of the JTWT.

Item	Performance
Mach Number	0.1 to 1.4
Max. Reynolds Number	$20 \times 10^6$ [1/m]
Stagnation Pressure	50 to 140 [kPa]
Stagnation Temperature	35 to 60 [°C]
Test Section Size	$2 \times 2 \times 4.13$ [m]
Construction	1960

### III. Experimental Description

#### A. Model Description

The model used in the current investigation is an 80% scaled NASA CRM. The size corresponds to 2.16% of the NASA CRM original design shape. The 80% scaled model is manufactured for our wind tunnel so that the ratio of the model to test section size is approximately equal to that of the NTF. The model configuration consists of a contemporary supercritical transonic wing and a fuselage that is representative of a widebody commercial transport aircraft. The CRM is designed for a cruise Mach number of  $M = 0.85$  and a corresponding design lift coefficient of  $C_L = 0.5$ . The aspect ratio is 9.0, the leading edge sweep angle is 35 deg, the wing reference area,  $S_{ref}$ , is  $0.179\text{m}^2$ , the wing span,  $b$ , is 1.2693m, and the mean aerodynamic chord,  $c$ , is 0.1513m. The model moment reference center is located 676.7mm downstream from the fuselage nose and 23.7mm below the fuselage centerline.

The model surface has 370 pressure orifices, which are 325 orifices on both the left and right wings, 12 orifices on fuselage, and 33 orifices on horizontal wings. The orifices on the wings are located in 9 span-wise wing stations ( $\eta = 0.131, 0.201, 0.283, 0.397, 0.502, 0.603, 0.727, 0.846, \text{ and } 0.950$ ) on both wings, and 1 span-wise wing station ( $\eta = 0.312$ ) on the left lower surface. The orifices on the horizontal wings are located 3 span-wise stations on the left upper surface and the right lower surface.

Five different configurations can be tested with the model: the wing/body (WB) alone, wing/body/pylon/nacelle (WBPN), wing/body/tail= $0^\circ$  (WBT0), wing/body/tail= $+2^\circ$  (WBT+2) and wing/body/tail= $-2^\circ$  (WBT-2). All configurations can be supported with a blade sting and a straight sting.



Figure 2. The 80% scaled NASA CRM model installed in the test section.

### B. Test Conditions

Wind tunnel tests are conducted with the model configuration of wing/body/tail= $0^\circ$  with the blade sting at the Cart#4 with porous walls for about one month. The data are obtained at  $M_{pc}=0.7, 0.83, 0.85, 0.856, 0.86,$  and  $0.87$  at  $P_0=60\text{kPa}$  and  $120\text{kPa}$ .  $Re_c$  corresponds to 2.27 million at  $M_{pc}=0.85$  and  $P_0=120\text{kPa}$ , and 1.14 million at  $M_{pc}=0.85$  and  $P_0=60\text{kPa}$ .  $Re_c$  values represented in this paper are based on the mean aerodynamic chord. Data are obtained with model angle of attack range from  $-3^\circ$  to  $10^\circ$ .

Boundary layer transition from laminar to turbulent flow need to be ensured to compare CFD data and wind tunnel tests data at the NTF and the Ames 11-ft. To fix transition on the model, vinyl trip dots, which are 0.05 inches in diameter, and 0.1 inches apart from center to center, are used for the investigation. A trip dot height of 0.0039 inches is used from the SOB (side of body) to yehudi break, 0.0035 inches is used from the yehudi break to the midwing and 0.0031 inches was used from the midwing to the wing tip. These trip dots are installed at 10% chord on both the upper and lower wings. A trip dot height of 0.0031 inches is applied at 0.15% length after of the nose on the fuselage. A trip dot height of 0.0031 is applied at 10% cord on both the upper and lower horizontal tails.

### C. Measurement items

Forces and moments, a model inclination, and surface pressures are measured. Forces and moments of the aerodynamic loads acting on the model are measured with an internal strain-gage balance. Pressure distributions on the model surface are measured with five modules of the Electronically Scanned Pressure (ESP) with the Digital Temperature Compensation (DTC). Moreover, model deformation measurement and infrared radiation measurement for the detection of boundary layer transition are also conducted.

To correct and investigate effects of the support and the wall interference, longitudinal pressure distributions of the centerline on the upper, side, lower walls are measured with five modules of the ESP. Wall pressure distribution measurements are also conducted with two configurations, which are the sting only installed in the test section without the model, and the empty test section without the model and the sting.

## IV. Application of balance calibration matrix conducted under near wind tunnel temperature

### A. JAXA automatic balance calibration machine description

A balance calibration for the wind tunnel test was conducted with the JAXA automatic balance calibration machine using combined loadings (Figure 3), which was constructed in 2010. The maximum load of the normal force is 10000N. Combined six-component loads are applied to a balance automatically with six electric actuators, and each load is measured with high precision load cell. To maintain load direction properly, repositioning system is adopted as the location and attitude control system. The positions are measured with high precision laser displacement meters. The position and attitude are controlled rapidly with motion base parallel rink system. The position tolerance is  $10\mu\text{m}$  and attitude tolerance is 0.002 degrees.

One special feature of the JAXA's automatic balance calibration machine is high-accuracy temperature control capabilities. Temperatures of entire equipments can be strictly controlled, because the balance, the position control system and the loading system are deformed according to temperature changes and distributions. Additionally, balance calibration can be conducted under near wind tunnel conditions. Temperature distributions across the

balance can be independently controlled within a range of 10 to 50 degrees centigrade to simulate temperature changes of the airflow produced by the JTWT. Moreover, a set of balance calibration is completed in a few days including preparation and back down.



Figure 3. JAXA automatic balance calibration machine.

### B. Effects of balance temperature on aerodynamic data

Differences between  $C_D$ ,  $C_L$ , and  $C_m$  calculated with balance calibration matrix at 50 degrees centigrade and those calculated with matrix at 23 degrees centigrade are plotted in Figure 4. The difference in  $C_D$  is about -2 to -13 drag counts, and the difference in  $C_L$  is up to -0.008. It seems that the effects of balance temperature differences between room temperatures and wind tunnel temperatures correspond to 1% of measured values approximately. The CRM tests are conducted to keep the balance temperature 50 degrees centigrade, and the balance calibration matrix at 50 degrees centigrade is, therefore, applied to all measured balance data.

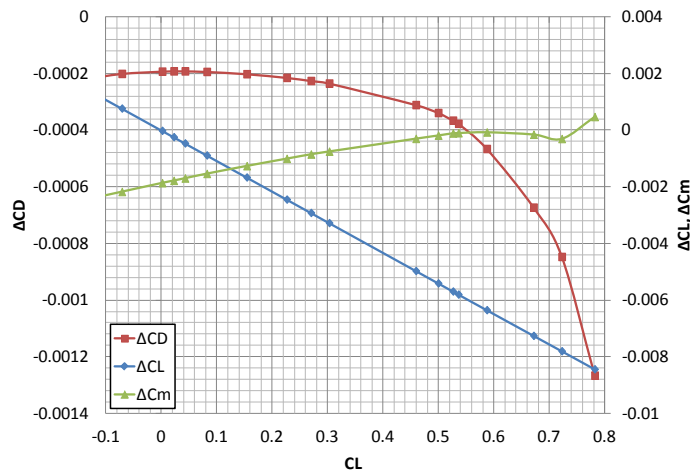


Figure 4. Errors of balance output due to balance calibration temperature.

## V. Fundamental wind tunnel interference correction

### A. Fundamental wind tunnel interference correction method

To correct fundamental wind tunnel interferences, correction amounts of the test section Mach number at the model center, the clear tunnel buoyancy, the wall interference, and the upflow are calculated following the

procedure shown in Figure 5. Each correction method is discussed in detail below. At first, the test section Mach number at the model center is calculated with the centerline static pressure probe data. Next, clear tunnel buoyancy is also calculated with the centerline probe data. Next, correction amounts of the wall interference are calculated with the Mach number and aerodynamic coefficients corrected for test section Mach number. Finally, the upflow angle is calculated with aerodynamic coefficients and angles of attack.

To apply the correction amounts to flow conditions and aerodynamic coefficients measured at the wind tunnel, each correction amounts for the Mach number, the angle of attack, and the buoyancy are summed respectively as shown in the right procedure of Figure 5. Firstly, the  $M_{pc}$  is corrected with the test section Mach number at the model center and the Mach number difference derived from the wall interference correction. The change in the Mach number affects the dynamic pressure, so that measured aerodynamic coefficients are corrected for the change in the dynamic pressure. Next, the angle of attack is corrected with the upflow angle and the flow angularity derived from the wall interference correction. Accordingly,  $C_D$  and  $C_L$  are corrected for the change in the angle of attack. Finally, in buoyancy correction,  $C_D$  is corrected with the clear tunnel buoyancy derived from the centerline probe and the buoyancy derived from the wall interference correction.

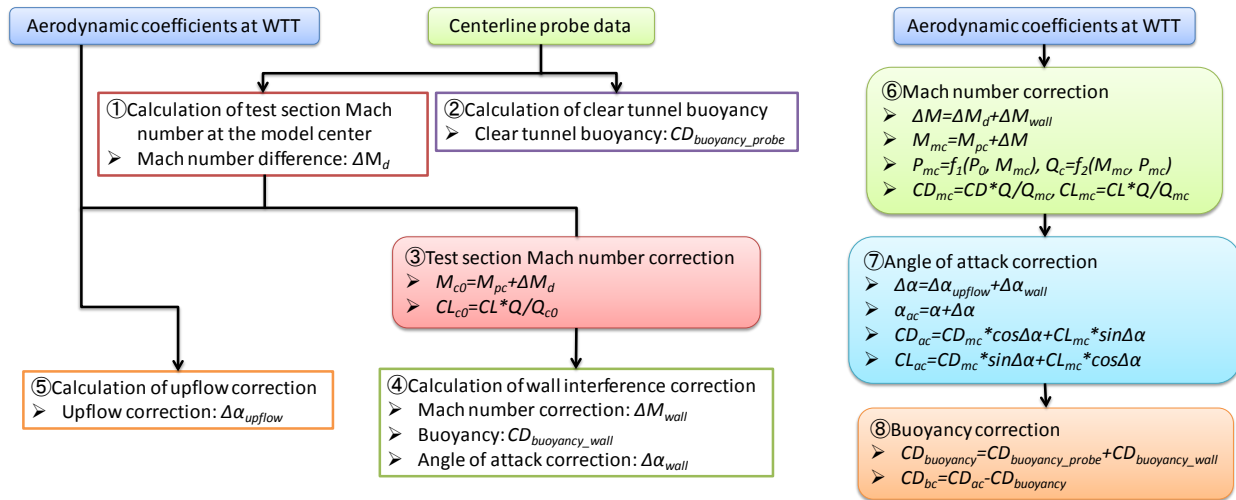


Figure 5. Fundamental wind tunnel interference correction.

### B. Test section Mach number correction at the model center

In the JTWT,  $M_{pc}$  calculated with  $P_0$  and  $P_{pc}$  is conventionally used to control the test section Mach number. To calculate test section Mach numbers at the model center from  $M_{pc}$ , pressure distributions along the centerline in the test section are measured with a short centerline probe<sup>10</sup>. The probe installed in the Cart#4 is shown in Figure 6, and pressure distributions are shown in Figure 7. Test section Mach numbers are corrected with Mach number differences between local Mach numbers at the model center measured with the probe and  $M_{pc}$ .

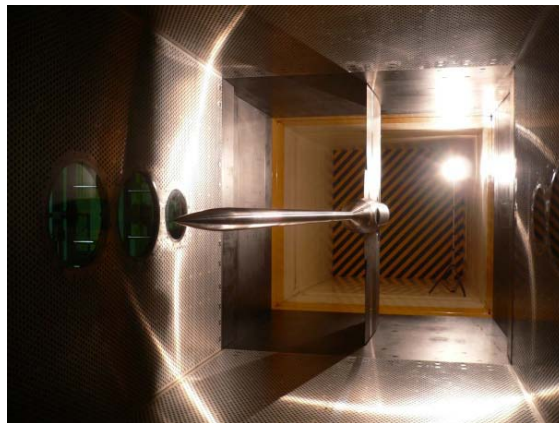


Figure 6. Short centerline probe installed in Cart#4.

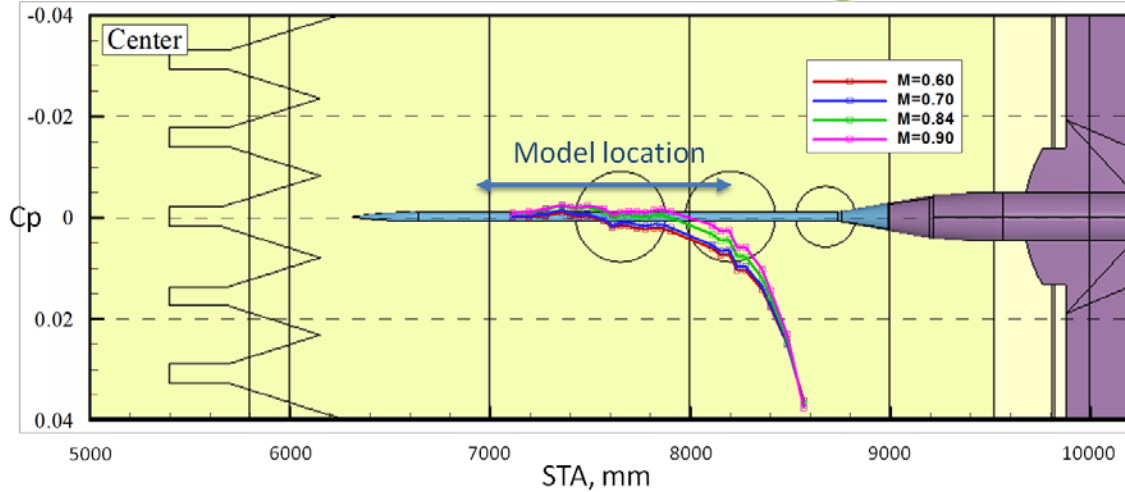


Figure 7. Pressure distributions measured with the short centerline probe in Cart#4.

### C. Clear tunnel buoyancy correction

To correct effects of the sting-strut system interference on the model, the clear tunnel buoyancy at the model location is also corrected with the pressure distributions. The buoyancy correction to be subtracted from  $C_D$  is derived as follows:

$$C_{D\_buoyancy} = -\frac{1}{S_{ref}} \int_{x_{nose}}^{x_{tail}} \left( \frac{dC_{p\_center}(X)}{dx} \times S_{Model}(X) \right) dx \quad (1)$$

The equation means the buoyancy of the model whole area, which is calculated with pressure distributions on the centerline probe measured by the probe. The buoyancy can be calculated before fabrication of the model and the sting. Thus, the blade sting length is designed not to be affected by the buoyancy. Buoyancies of the CRM model are from -4 to -1 drag counts with a Mach number range from 0.7 to 0.87.

### D. Wall interference correction

To correct wall interference effects, Mokry's method<sup>2</sup> is applied to data measured at the JTWT with porous walls. In the method, airflow in the wind tunnel is represented by the disturbance velocity potential, which is superposition of the model disturbance potential and the wall interference potential, in the finite-length cylindrical domain. The boundary conditions are obtained by pressure distributions on the upper, lower, and side walls measured at the same time as forces and moments. From wall interference velocity, changes in Mach numbers and angles of attack distributions are calculated at the model location.

With the changes, measured test conditions and aerodynamic data are corrected. At first, aerodynamic forces and moments coefficients are corrected by changes in dynamic pressure and static pressure associated with the Mach number correction. Next, pressure gradients in the freestream direction cause buoyancy forces.  $C_D$  is corrected by Mach number distributions. Moreover,  $C_L$  and  $C_D$  should be obtained in the directions normal and parallel to the corrected stream velocity vector. The angle corrections to  $C_L$  and  $C_D$  are applied to obtain corrected data for the wall interference finally.

Measured pressure distributions on the upper, side, and lower walls at  $M_{pc}=0.85$  and  $\alpha=3.0$  degrees are shown in Figure 8. These pressures measured at the empty test section are subtracted from data measured with the CRM model at the test section. The pressure distribution on the upper wall has a suction peak around the model due to the low pressure above the wing, and another peak at the junction of the sting and the sting pod. Another peak is derived from the subtraction of pressures measured at empty test section. The pressure distribution on the lower wall becomes high, because the wall interferes with downwash flow coming from the model. From the pressure distributions, Mach number distributions and angle of attack distributions around the model are obtained by Mokry's method as shown in Figure 9.

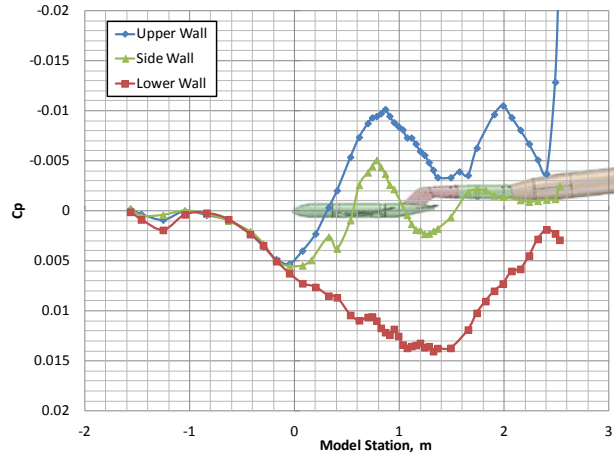


Figure 8. Pressure distributions on the upper, side, and lower walls at an attack angle of 3.0 degrees.

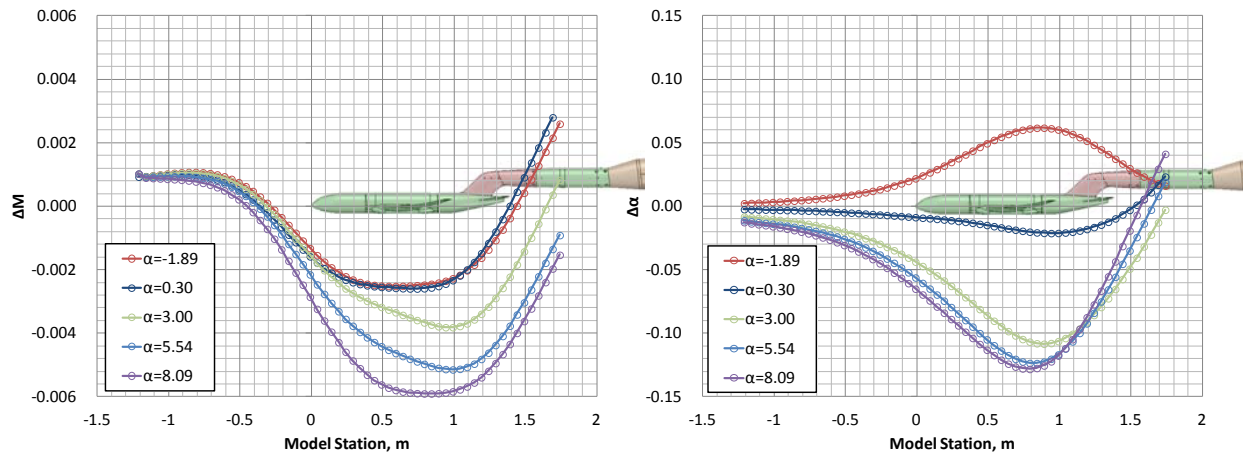


Figure 9. Mach number and flow angularity distributions obtained by the wall interference correction.

### E. Upflow angle correction

To correct flow angularity in the test section, forces and moments data with the model inverted are measured. Upflow angles are calculated by the upright and inverted model lift curves against angles of attack through a specific lift coefficient range around  $C_L=0$ . The difference of attack angle is 0.08 degrees at  $M_{pc}=0.85$ , so the upflow angle is 0.04 degrees.

## VI. Correction results of fundamental wind tunnel interference

### A. Correction results of fundamental wind tunnel interference

Correction amounts of the Mach number, the angle of attack, and the buoyancy drag coefficient in the fundamental wind tunnel interference are shown in Figure 10. Each correction effects of the test section Mach number at the model center, the clear tunnel buoyancy, the wall interference, and the upflow are included. The total Mach number correction is from -0.002 to -0.006. The total angle of attack correction is almost from -0.1 to 0.1 degrees. The total buoyancy correction is from -5 to -1 drag counts.

Correction amounts of  $C_D$  and  $C_L$  calculated from the Mach number and angles of attack, and buoyancy drag corrections are shown in Figure 11. In the corrections for  $C_D$ , correction amounts of the wall interference and the upflow angle are relatively large. The sum of corrections for  $C_D$  is from -2 to 3 drag counts and those at  $C_L=0.5$  is within 1 drag counts. In the corrections for  $C_L$ , correction amounts of wall interference are large. The effect of wall interference increases with increasing  $C_L$ . The sum of corrections for  $C_L$  is from -0.001 to 0.005.

The fundamental wind tunnel interference correction method is applied to the measured data.  $C_L$  against  $C_D$  is compared between measured data and corrected data at  $M_{pc}=0.85$  and  $Re_c=2.27$  million as shown in Figure 12. Results show that differences between uncorrected data and corrected data of  $C_L$ - $C_D$  polar curve are relatively small at the wind tunnel. The difference in  $C_D$  at  $C_L=0.5$  is 1.4 drag counts approximately.

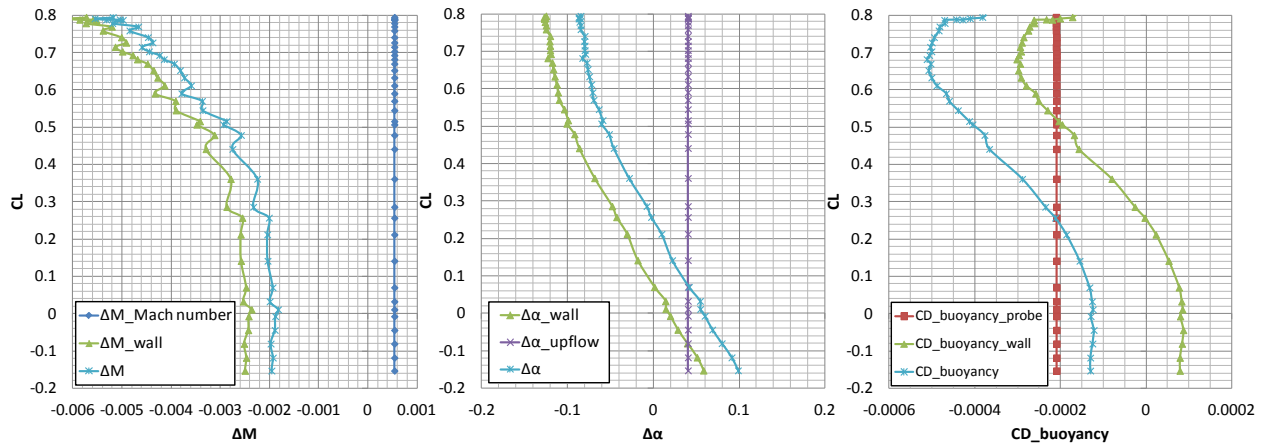


Figure 10. Correction amounts of Mach number, angle of attack, and buoyancy drag coefficients at  $M_{pc}=0.85$ .

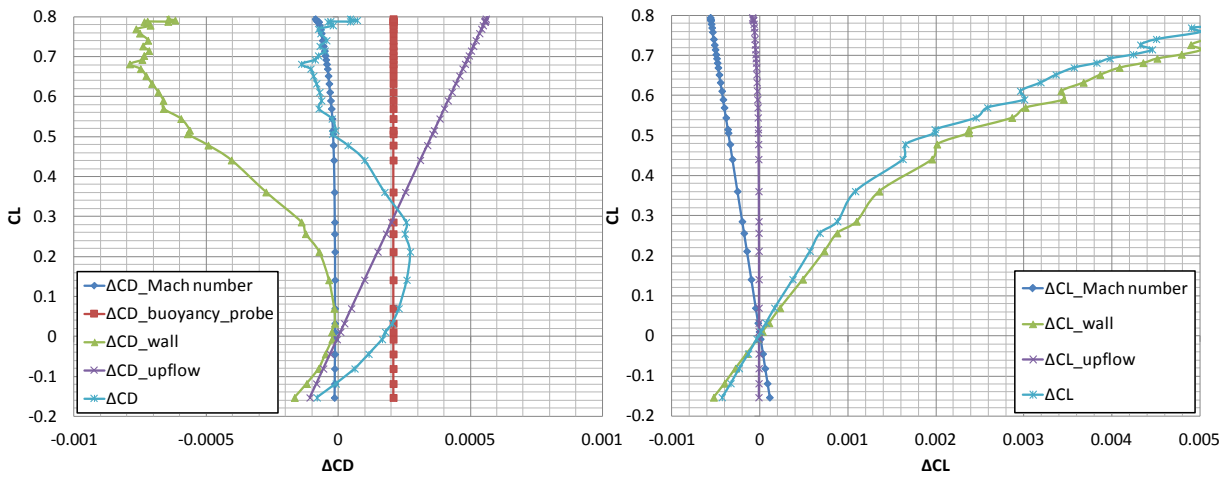


Figure 11. Correction amounts of  $C_D$  and  $C_L$  derived from the fundamental wind tunnel interference at  $M_{pc}=0.85$ .

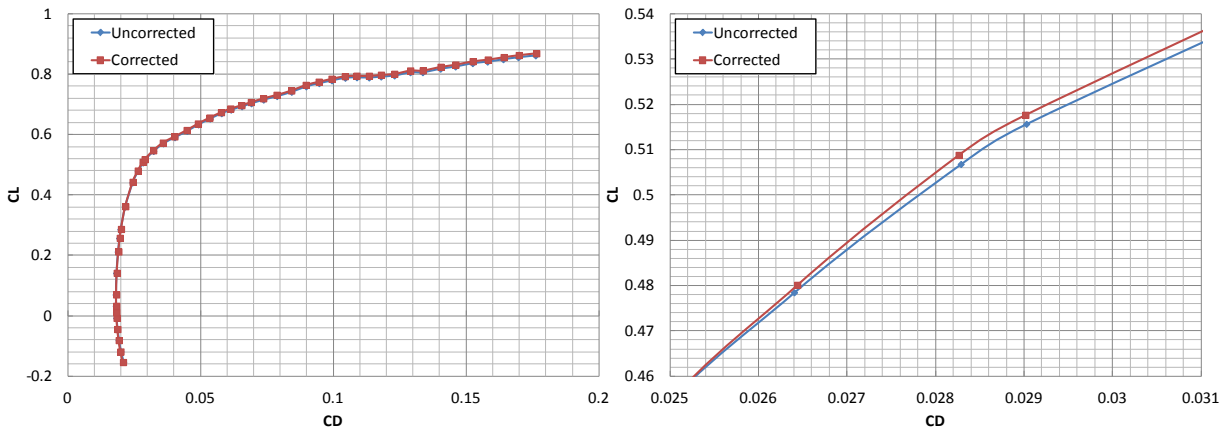


Figure 12. Comparisons of  $C_L$  and  $C_D$  between measured data and corrected data at  $M_{pc}=0.85$  and  $Re_c=2.27$  million.

## B. Comparisons of wall interference correction amounts with those of the NTF and the Ames 11-ft

Correction amounts of the Mach number, the angle of attack,  $C_D$ , and  $C_L$  derived from each wall interference correction method are compared with those of the NTF and the Ames 11-ft as shown in Figure 13. In the correction of the Mach number, the data in the JTWT and in the Ames 11-ft is negative amounts, while the data in the NTF are positive amounts. In the correction for the angle of attack, the absolute values of the data in the JTWT are larger than those in the NTF and the Ames 11-ft, though all data has the same tendency.

In the correction for  $C_D$ , the data in the JTWT and the data in the Ames 11-ft show the same tendency. The data in the NTF show the opposite tendency. Besides, in the correction for  $C_L$ , all the data show the same tendency. The amounts of the data in the JTWT are almost four times the amounts of the data in the NTF, and ten times of the Ames 11-ft. These differences are caused by the differences in the corrections for the angle of attack of them.

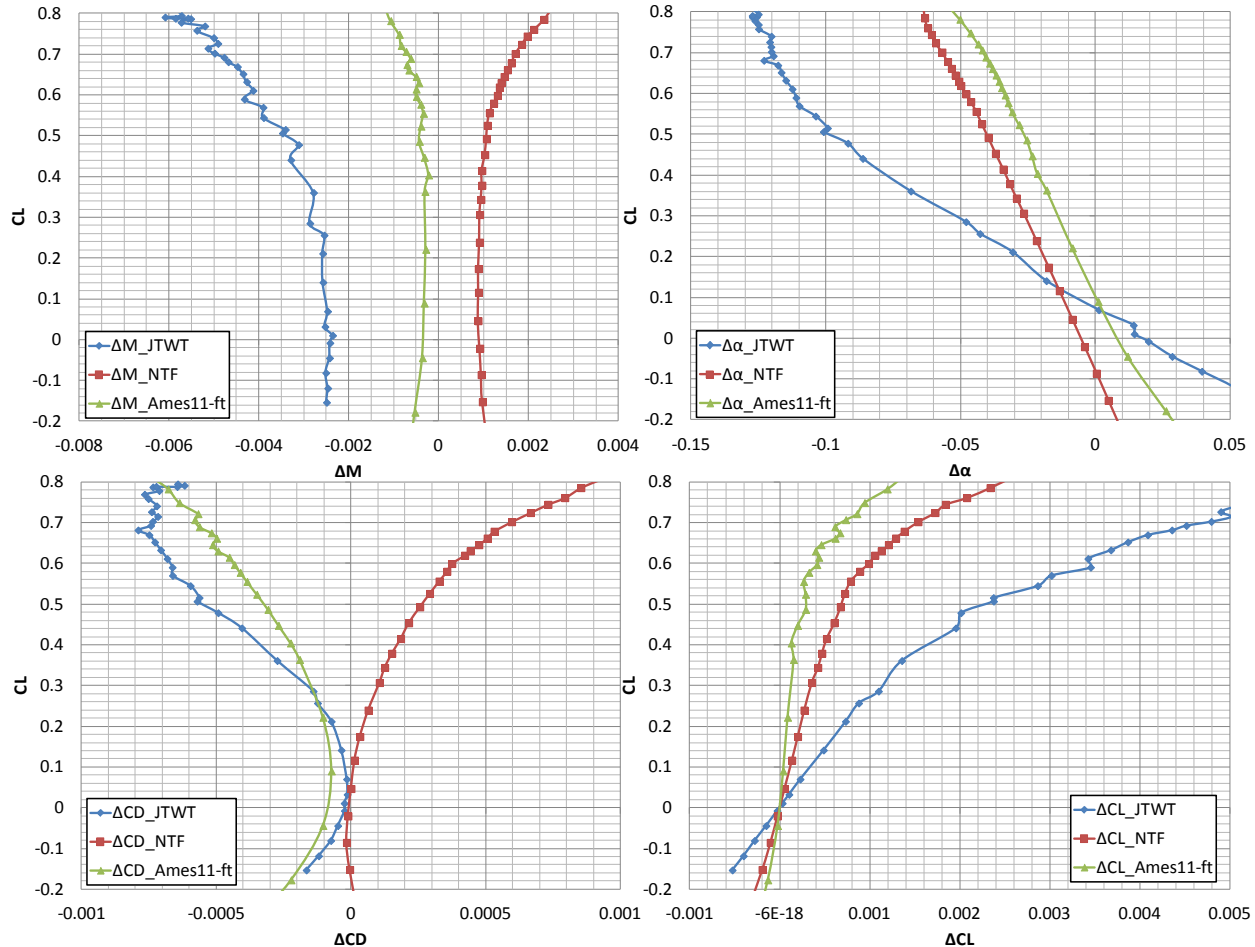


Figure 13. Comparisons in corrections of Mach number, angle of attack,  $C_D$ , and  $C_L$  derived from wall interference correction with those of the NTF, and the Ames 11-ft.

## VII. Corrected WTT data and support interference analysis with CFD

### A. Computational method and condition

CFD analysis is conducted with TAS (Tohoku university Aerodynamic Simulation) code in this study. The code is a well-validated code and used in a variety of aerospace applications in the JAXA. In the TAS, full Navier-Stokes equations are solved on the unstructured grid by a cell-vertex finite volume method. As a turbulence model, the Spalart-Allmaras model<sup>11</sup> is used. The flow on the model surfaces is calculated as fully turbulent flow in this study.

Two grids of the wing/body/tail= $0^\circ$  with the blade sting and the wing/body/tail= $0^\circ$  without the blade sting are conducted as shown in Figure 14. To compare with our wind tunnel data, a freestream Mach number of 0.85 and  $Re_c=2.27$  million based on mean aerodynamic chord are calculated. Angles of attack of 0, 1, 2, 3, 4, and 5 degrees are selected.

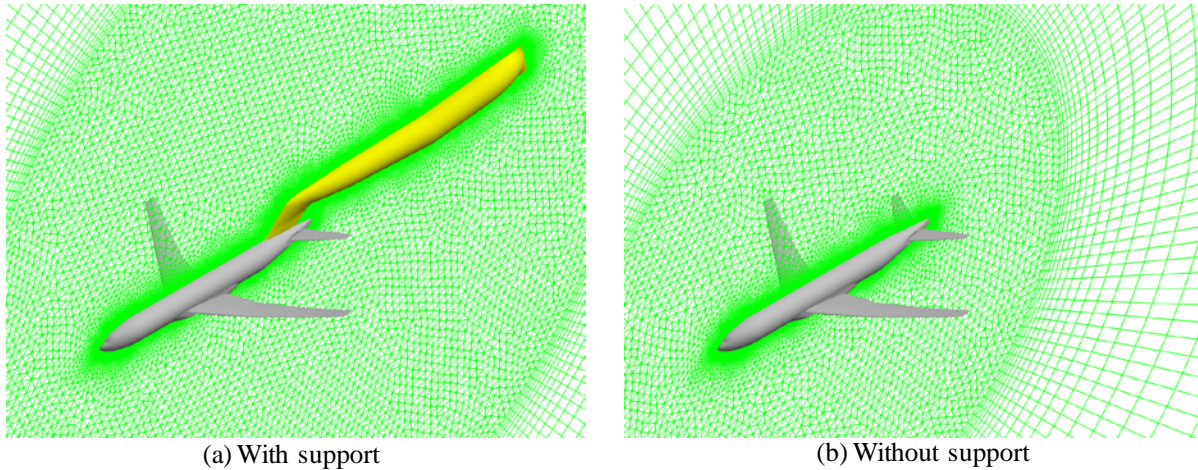


Figure 14: Computational cases of the CRM with support and the CRM without support.

### B. Comparisons of corrected WTT data with CFD data and investigations of support interference by CFD

$C_D$  and  $C_L$  against angle of attack are compared between the corrected WTT data and the CFD data with support at a freestream Mach number of 0.85 and  $Re_c=2.27$  million as shown in Figure 15. Mach numbers of the corrected WTT data are changed from  $M_{pc}=0.85$  to corrected Mach numbers, so that the corrected WTT data at corrected Mach numbers of 0.85 are interpolated linearly with the corrected WTT data at  $M_{pc}=0.856$ . The difference in  $C_D$  at low angle of the model is about 5 drag counts, and the difference increases with increasing the angle of attack. The wing deformation effect is one of the reasons for the increase. The  $C_L$  of WTT is less than that of the CFD with support at all angles. The difference corresponds to an angle of attack of about 0.2 degrees. It seems that the angularity is probably caused by an inclination of 6.43 degrees of sting-strut system to the model attitude.

In these figures, the CFD with support and the CFD without support are also compared to investigate support interference effects.  $C_D$  and  $C_L$  of the CFD with support is less than those of the CFD without support, so that effects of support interference decrease  $C_D$  and  $C_L$ . Contours of pressure distributions differences on the upper surface and on the vertical symmetry plane to the model obtained by subtracting the CFD without support from the CFD with support are illustrated in Figure 16. Effects of the blade sting move shock waves on the wings upstream. This means that Mach numbers in wings are decreased by the increase in pressure at the sting. As the result, the  $C_D$  and the  $C_L$  are decreased by the support interference. Moreover, pressures at upstream of the connection of blade sting and the upper surface of the rear end of the fuselage and the horizontal tail are increased. These increases in the pressure caused by the lower surface of the blade sting decrease  $C_L$  and increase  $C_m$ . Furthermore, the right figure shows that Mach number distributions in the large area around the model are decreased by the effect of the blade sting.

### C. Comparisons of support interference effects calculated by CFD with those of the NTF

To confirm support interference effects calculated by CFD, differences in  $C_D$ ,  $C_L$ , and  $C_m$  obtained by subtracting CFD without support from CFD with support are compared with those of the NTF<sup>12</sup> as shown in Figure 17. The calculated condition of  $Re_c=5$  million is also analyzed at the JTWT. The results show that Reynolds number effects on the support interference are negligibly small at an angle of attack of 4 degrees or less. Effects of the blade sting of the JTWT and the NTF show almost the same tendency, and the amounts of the effect on  $C_D$  are 20 to 40 drag counts. Thus, the configuration of the blade sting has a considerable effect on the measured WTT data. The effects of the JTWT are less than that of the NTF relatively, because the sting length of the JTWT is shorter, and the thickest part of the sting of the JTWT is slimmer than that of the NTF.

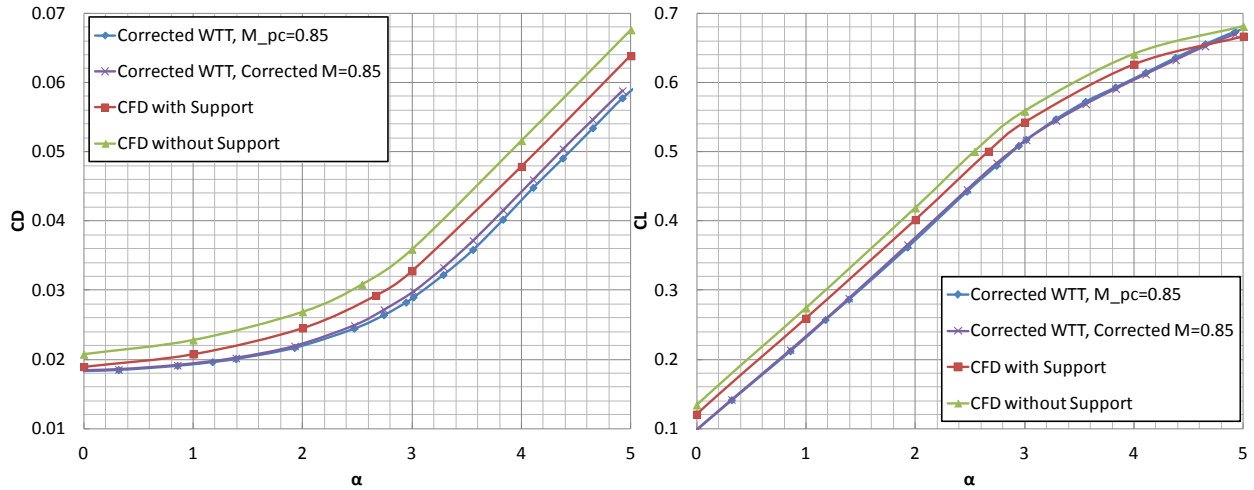


**Figure 15. Comparisons of corrected WTT data with CFD data with support and investigations of support interference.**

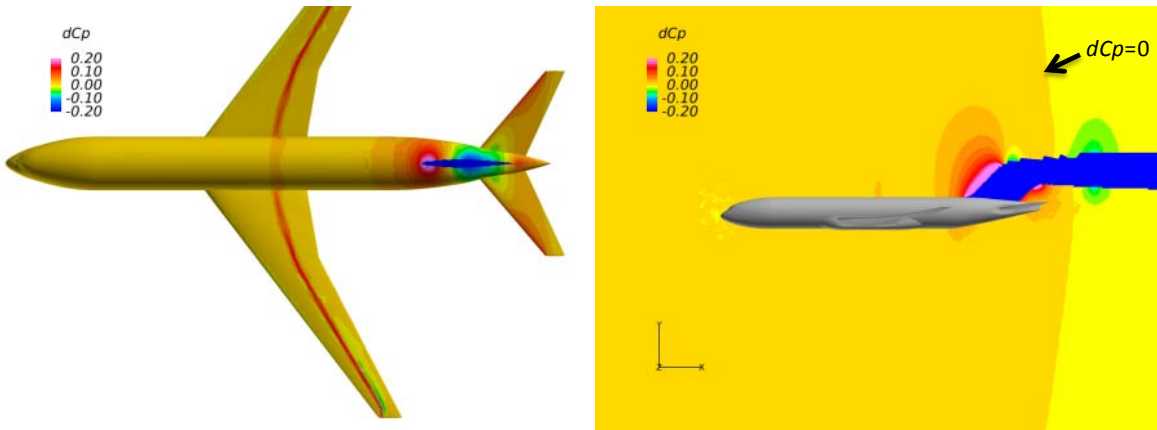


**Figure 16. Contours of pressure distributions differences on the upper surface and on the vertical symmetry plane to the model obtained by subtracting CFD without support from CFD with support at  $M=0.85$  at  $Re_c=2.27$  million.**

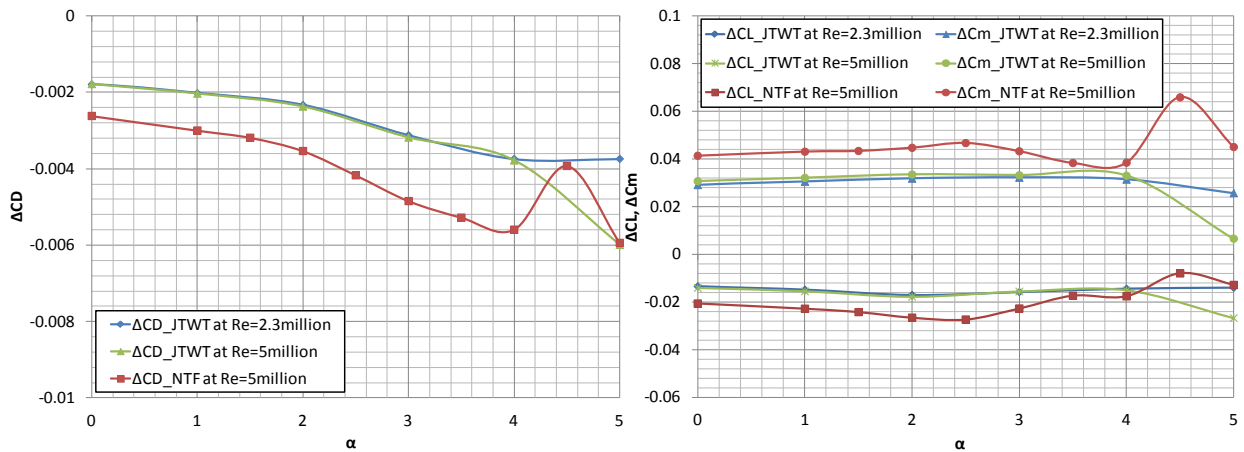


**Figure 17. Comparisons of differences between CFD with support and CFD without support with those of the NTF.**

## VIII. Conclusion

It is confirmed that the errors of balance output due to balance calibration temperature and the correction amounts of the fundamental wind tunnel interference including the test section Mach number correction, the clear tunnel buoyancy, the wall interference correction, and the upflow angle correction. The correction method is integrated and applied to WTT data. Results show that the sum of corrections for  $C_D$  at  $C_L=0.5$  is within 1 drag counts, and the difference in  $C_D$  at  $C_L=0.5$  between the uncorrected and the corrected  $C_L C_D$  polar curve is 1.4 drag counts. Moreover, amounts of wall interference correction are compared with those of the NTF and the Ames 11-ft.

The WTT data corrected for the fundamental wind tunnel interference at a corrected Mach number of 0.85 are compared with the CFD data with support. Moreover, support interference effects of the blade sting are investigated with comparisons of the CFD with support and the CFD without support. Effects of the blade sting are also compared with those of the NTF. These data have almost the same tendency, and the amounts of the effect on  $C_D$  are 20 to 40 drag counts. Thus, these results show that aerodynamic data, which are not affected by wind tunnel, can be estimated more precisely by the application of the balance calibration matrix, the fundamental wind tunnel interference correction, and the support interference correction appropriately.

## Acknowledgments

The authors would like to thank Ms. Mellissa B. Rivers of NASA Langley Research Center for her providing of the NASA CRM model information and wind tunnel and CFD results. The authors would like to thank Dr. Kazuomi Yamamoto, Dr. Mitsuhiro Murayama, Mr. Kentaro Tanaka, and Mr. Tohru Hirai for their support of wind tunnel CFD analysis. The authors would like to thank the staffs of the Transonic Wind Tunnel Section for their help in conducting experiments.

## References

- <sup>1</sup>Ulbrich, N., "The Application of Panel Method Code ANTARES to Wind Tunnel Wall Problems," AIAA 2002-0307.
- <sup>2</sup>Mokry, M., "Subsonic Wall Interference Corrections for Finite-Length Test Sections Using Boundary Pressure Measurements," Proceedings of the Fluid Dynamics Panel Specialists' Meeting, 1982, pp.10.1-10.5, AGARD CP-335.
- <sup>3</sup>Kohzai, M., Sudani, N., Yamamoto, K., Ueno, M., and Hashimoto, A., "Experimental and Numerical Studies of Support Interference in the JAXA 2m x 2m Transonic Wind Tunnel," AIAA 2010-4200.
- <sup>4</sup>Hashimoto, A., Aoyama, T., Kohzai, M., and Yamamoto, K., "Transonic Wind Tunnel Simulation with Porous Wall and Support Devices," AIAA 2010-4201.
- <sup>5</sup>Hashimoto, A., Kohzai, M., "Wall Interference Analysis by Whole Wind Tunnel CFD," 5th Symposium on Integrating CFD and Experiments in Aerodynamics, 2012.
- <sup>6</sup>Levy, D. W., Zickuhr, T., Vassberg, J., Agrawal, S., Wahls, R. A., Pirzadeh, S., and Hemsch, M. J., "Data Summary from the First AIAA Computational Fluid Dynamics Drag Prediction Workshop," Journal of Aircraft, Vol. 40, No. 5, 2003, pp. 875-882.
- <sup>7</sup>Vassberg, J. C., DeHaan, M. A., Rivers, M. B., and Wahls, R. A., "Development of a Common Research Model for Applied CFD Validation Studies," AIAA 2008-6919.
- <sup>8</sup>Rivers, M. B., and Dittberner, A., "Experimental Investigations of the NASA Common Research Model in the NASA Langley National Transonic Facility and NASA Ames 11-Ft Transonic Wind Tunnel," AIAA 2011-1126.
- <sup>9</sup>Ueno, M., Kohzai, M., Koga, S., Kato, H., Nakakita, K., Sudani, N., "80% Scaled NASA Common Research Model Wind Tunnel Test of JAXA at Relatively Low Reynolds Number," AIAA paper, AIAA 51<sup>st</sup> Aerospace Sciences Meeting, Grapevine, Texas, 7-10 January 2013.
- <sup>10</sup>Kohzai, M., Ueno, M., Shiohara, T., Sudani, N., "Calibration of the test section Mach number in the JAXA 2m x 2m Transonic Wind Tunnel," AIAA 2008-848.
- <sup>11</sup>Spalart, P. R. and Allmaras, S. R., "A One-Equation Turbulence Model for Aerodynamic Flows," AIAA 1992-0439, 1992.
- <sup>12</sup>Rivers, M. B., and Hunter, C. A., "Support System Effects on the NASA Common Research Model," AIAA 2012-0707.